Available online at www.sciencedirect.com
ScienceDirect
Journal of the European Ceramic Society 30 (2010) 2017–2030
www.elsevier.com/locate/jeurceramsoc

Effect of Al_2O_3 and K_2O content on structure, properties and devitrification of glasses in the Li_2O–SiO_2 system

Hugo R. Fernandes [a], Dilshat U. Tulyaganov [a,b], Ashutosh Goel [a], Manuel J. Ribeiro [c], Maria J. Pascual [d], José M.F. Ferreira [a,*]

[a] *Department of Ceramics and Glass Engineering, University of Aveiro, CICECO, 3810-193 Aveiro, Portugal*
[b] *Turin Polytechnic University in Tashkent, 17 Niyazova str., 100174 Tashkent, Uzbekistan*
[c] *UIDM, ESTG, Polytechnic Institute of Viana do Castelo, 4900 Viana do Castelo, Portugal*
[d] *Instituto de Cerámica y Vidrio (CSIC), C/Kelsen 5, Campus de Cantoblanco, 28049 Madrid, Spain*

Received 4 August 2009; received in revised form 1 April 2010; accepted 10 April 2010
Available online 10 May 2010

Abstract

The effect of Al_2O_3 and K_2O content on structure, sintering and devitrification behaviour of glasses in the Li_2O–SiO_2 system along with the properties of the resultant glass–ceramics (GCs) was investigated. Glasses containing Al_2O_3 and K_2O and featuring SiO_2/Li_2O molar ratios (3.13–4.88) far beyond that of lithium disilicate ($Li_2Si_2O_5$) stoichiometry were produced by conventional melt-quenching technique along with a bicomponent glass with a composition $23Li_2O$–$77SiO_2$ (mol.%) ($L_{23}S_{77}$). The GCs were produced through two different methods: (a) nucleation and crystallization of monolithic bulk glass, (b) sintering and crystallization of glass powder compacts.

Scanning electron microscopy (SEM) examination of as cast non-annealed monolithic glasses revealed precipitation of nanosize droplet phase in glassy matrices suggesting the occurrence of phase separation in all investigated compositions. The extent of segregation, as judged from the mean droplet diameter and the packing density of droplet phase, decreased with increasing Al_2O_3 and K_2O content in the glasses. The crystallization of glasses richer in Al_2O_3 and K_2O was dominated by surface nucleation leading to crystallization of lithium metasilicate (Li_2SiO_3) within the temperature range of 550–900 °C. On the other hand, the glass with lowest amount of Al_2O_3 and K_2O and glass $L_{23}S_{77}$ were prone to volume nucleation and crystallization, resulting in formation of $Li_2Si_2O_5$ within the temperature interval of 650–800 °C.

Sintering and crystallization behaviour of glass powders was followed by hot stage microscopy (HSM) and differential thermal analysis (DTA), respectively. GCs from composition $L_{23}S_{77}$ demonstrated high fragility along with low flexural strength and density. The addition of Al_2O_3 and K_2O to Li_2O–SiO_2 system resulted in improved densification and mechanical strength.

Keywords: Sintering; Microstructure-final; Glass; Glass–ceramics; Lithium disilicate

1. Introduction

Phase separation, nucleation and crystallization of glasses in the Li_2O–SiO_2 system have been the subject of many theoretical studies.[1–9] According to Vogel,[9] Li_2O–SiO_2 liquids containing less than 30 mol.% Li_2O lead to opalescent or opaque glasses on cooling owing to phase separation. TEM investigation revealed segregation into droplet like zones of Li-rich phase and SiO_2-rich glass matrix. Moreover, within the Li_2O content range of 14–16 mol.% in the entire glass, $Li_2Si_2O_5$ (here after referred as LD) composition was already reached in the droplet phase.[9] Further increasing the Li_2O content in the entire glass reduced the surface tension of the two phases because Li_2O entered into the SiO_2-rich phase surrounding the droplets and the size of the droplets reduced continuously. Subsequently, with Li_2O content of 33.3 mol.%, corresponding to $Li_2Si_2O_5$ in the entire glass, the droplet phase and the phase surrounding the droplets had the same composition, with this stoichiometric LD glass composition exhibiting the most homogeneous possible structure.

Generally, slight changes in lithium silicate glass composition may have significant effects on chronology and morphology of phases formed. The addition of P_2O_5 to LD glass was observed to induce amorphous phase separation and to increase the crystal nucleation rate, simultaneously.[1,2,10–12] The incorporation of

* Corresponding author. Tel.: +351 234 370242; fax: +351 234 370204.
E-mail address: jmf@ua.pt (J.M.F. Ferreira).

0955-2219/$ – see front matter © 2010 Elsevier Ltd. All rights reserved.
doi:10.1016/j.jeurceramsoc.2010.04.017

Table 1
Compositions of the experimental glasses.

	Oxides (mol.%)				
	SiO_2/Li_2O	Li_2O	K_2O	Al_2O_3	SiO_2
G1	4.88	15.23	5.24	5.24	74.30
G2	3.83	19.08	3.94	3.94	73.04
G3	3.13	22.96	2.63	2.63	71.78
$L_{23}S_{77}$	3.35	22.96	-	-	77.04

TiO_2 in addition to P_2O_5 greatly affected phase evolution, morphology and thereby thermo-physical properties of crystallized glasses in low alumina Li_2O–SiO_2 glasses.[13] The conventional nucleating agent ZrO_2 in Li_2O–SiO_2 glass enhanced the polymerization of the silicate network, and caused a significant red shift in Raman frequencies for Q^2 species and amorphous phase separation before crystallization.[14] Recently it was demonstrated that very small amount of MnO_2 and V_2O_5 (less than 1 wt.% in total) might decrease the critical cooling rate of the LD melt and so increase the glass forming tendency.[15] The occurrence of this phenomenon was attributed to the following possible reasons: (a) an increase of melt viscosity and, therefore, of the kinetic barrier against crystallization; (b) an increase of the surface energy difference between the Li-silicate crystals and residual melt, thus enhancing the surface energy barrier against nuclei formation.[15]

The role of Al_2O_3 and K_2O on crystallization in glasses featuring SiO_2/Li_2O ratios (3.13–4.88) far beyond of LD stoichiometry was recently studied.[16] Glasses in both bulk and frit form were produced by the conventional melt-quenching technique using alumina crucibles. Therefore, an unavoidable alumina uptake from the crucibles cannot be neglected. To eliminate this anomaly leading to uncontrolled compositional variations, Pt crucibles were used in the present work to prepare the same glass compositions along a new bicomponent (23 mol.% Li_2O and 77 mol.% SiO_2) glass denoted as $L_{23}S_{77}$. The aim of this work was, therefore, to get a deeper insight on phenomena related to a metastable immiscibility and devitrification in Li_2O-SiO_2 glasses in relevance with Al_2O_3 and K_2O content. Particular emphasis was also given to the investigation of sintering behaviour and the properties of the corresponding glass powder compacts. Significant differences between $L_{23}S_{77}$ composition and its Al_2O_3 and K_2O containing counterparts were encountered in terms of structure, crystallization kinetics, thermal behaviour and properties.

2. Experimental procedure

Table 1 presents the compositions of the glasses investigated in the present study along with the corresponding SiO_2/Li_2O ratios. The addition of Al_2O_3 and K_2O was performed on equimolecular basis and the amount of additives decreased from glass G1 to G3. The glass $L_{23}S_{77}$ containing the same amount of Li_2O (22.96 mol.%) as glass G3, but richer in SiO_2 (77.04 mol.%) due to complete exclusion of Al_2O_3 and K_2O from its composition was also prepared and investigated for comparison purposes.

Powders of technical grade SiO_2 (purity > 99.5%) and of reactive grade Al_2O_3, Li_2CO_3, and K_2CO_3 were used. Homogeneous mixtures of batches (~100 g), obtained by ball milling, were calcined at 800 °C for 1 h and then melted in Pt crucibles at 1550 °C for 1 h, in air. Glasses were produced in bulk (monolithic) and frit form as described below.

2.1. Crystallization behaviour of bulk glasses

Two sets of bulk glasses for each composition were obtained by pouring the glass melt on preheated bronze mould. The first set of glasses was allowed to cool down in the air while second set of glasses was subjected to annealing at 450 °C for 1 h.

The coefficient of thermal expansion (CTE) of the annealed samples was determined by dilatometry using prismatic samples of bulk glasses with cross section of 3 mm × 4 mm (Bahr Thermo Analyse DIL 801 L, Germany; heating rate 5 K min^{-1}).

The onset of crystallization, T_c and peak temperature of crystallization, T_p for the investigated glasses was obtained from DTA thermographs of glass grains with sizes in the range of 415–1000 μm, collected by sieving of grounded non-annealed glass blocks. The DTA was carried out in air (Netzsch 402 EP, Germany) from room temperature to 1000 °C at different heating rates (β = 2, 5, 10 and 15 K min^{-1}). The kinetics of crystallization was studied using the formal theory of transformation kinetics as developed by Johnson and Mehl[17] and Avrami,[18–20] for non-isothermal processes:

$$\ln\left(\frac{T_p^2}{\beta}\right) = \frac{E_c}{RT_p} - \ln q = 0 \quad (1)$$

which is the equation of a straight line, whose slope and intercept gives the activation energy, E_c, and the pre-exponential factor, $q = Q^{1/n}K_0$, respectively, and the maximum crystallization rate by the relationship[21]:

$$\left.\frac{d\chi}{dt}\right|_p = 0.37\beta E_c n\left(RT_p^2\right)^{-1} \quad (2)$$

which enables obtaining, for each heating rate, a value of the kinetic exponent, n. In Eq. (2), χ corresponds to the crystallization fraction and $\left.\frac{d\chi}{dt}\right|_p$ is the crystallization rate, which may be calculated by the ratio between the ordinates of the DTA curve and the total area of the crystallization curve.

In order to study the evolution of crystallization phases in monolithic glasses, the annealed glasses were cut into cubes (1 cm × 1 cm × 1 cm) and heat treated non-isothermally at 550, 650, 750, 800 and 900 °C for 1 h, respectively, at heating rate of 2 K min^{-1}.

2.2. Sintering and crystallization of glass powder compacts

The glass frits were produced by quenching of melt in cold water. Further, the glass frits were dried and milled in high speed agate mill resulting in fine glass powders with mean particle size of 5–10 μm as determined by light scattering technique (Coulter LS 230, UK, Fraunhofer optical model). Infrared spectra of the

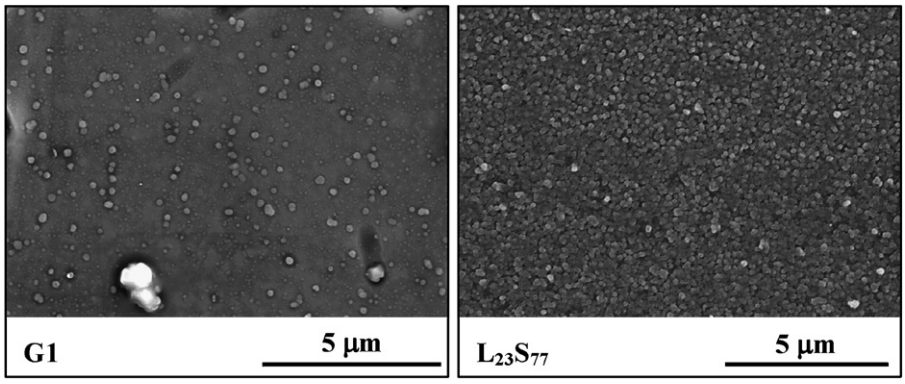

Fig. 1. SEM images of non-annealed bulk glasses G1 and $L_{23}S_{77}$.

glass powders were obtained using an infrared Fourier spectrometer (FTIR, model Mattson Galaxy S-7000, USA) in the range of 300–1500 cm^{-1}. For this purpose, each sample was mixed with KBr in the proportion of 1/150 (by weight) for 15 min and pressed into a pellet using a hand press.

A side-view hot-stage microscope Leitz Wetzlar (Germany) equipped with a Pixera video-camera and image analysis system was used to investigate the sintering behaviour of glass powder compacts. The measurements were conducted in air with a heating rate of 5 K min^{-1}. The cylindrical shaped samples from glass powder compacts with height and diameter of ≈3 mm were prepared by cold-pressing the glass powders. The cylindrical samples were placed on a 10 mm × 15 mm × 1 mm alumina (>99.5 wt.% Al_2O_3) support. The temperature was measured with a chromel–alumel thermocouple contacted under the alumina support. The temperatures corresponding to the characteristic viscosity points (first shrinkage (T_{FS}), maximum shrinkage (T_{MS}), softening (T_D), half ball (T_{HB}) and flow (T_F)) were obtained from the graphs and photomicrographs taken during the hot-stage microscopy experiment.[22,23]

Rectangular bars with dimensions of 4 mm × 5 mm × 50 mm were prepared by uniaxial pressing (40 MPa). The bars were sintered under non-isothermal conditions for 1 h at 800, 850 and 900 °C using a low heating rate of 2 K min^{-1} aimed to prevent deformation of samples.

Archimedes' method (i.e. immersion in diethyl phthalate) was employed to measure the apparent density of the samples. The three-point bending strength tests were performed on rectified parallelepiped bars (3 mm × 4 mm × 50 mm) of sintered GCs (Shimadzu Autograph AG 25 TA, 0.5 mm/min displacement): the results were obtained from at least 10 different independent samples.

2.3. Crystalline phase analysis and microstructural evolution in glass–ceramics

The amorphous nature of the parent glasses and the nature of crystalline phases present in the GCs were determined by X-ray diffraction (XRD) analysis (Rigaku Geigerflex D/Mac, C Series, Japan; Cu K_a radiation, $2\theta = 10–60°$ with a 2θ-step of 0.02 deg s^{-1}). The crystalline phases were identified by comparing the obtained diffractograms with patterns of standards complied by the International Centre for Diffraction Data (ICDD).

Microstructure observations were done at polished (mirror finishing) and then etched surfaces of samples (by immersion in 2 vol.% HF solution for 5–7 min) by field emission scanning electron microscopy (FE-SEM, Hitachi S-4100, Japan, 25 kV acceleration voltage, beam current 10 μA) under secondary electron mode.

3. Results

3.1. Microstructure and properties of glasses

Melting at 1550 °C for 1 h was adequate to obtain bubble free, transparent and colourless glasses G1, G2 and G3, while in case of $L_{23}S_{77}$ transparent melt transformed into a cloudy hazy glass on cooling. SEM images of as cast non-annealed samples presented in Fig. 1 revealed the precipitation of a nanosize droplet phase in glassy matrices suggesting the occurrence of liquid–liquid phase separation in all investigated compositions. However, the mean droplet diameter and the population density of droplets decreased by adding Al_2O_3 and K_2O into the Li_2O–SiO_2 system. Accordingly, homogeneous and transparent appearance was conferred to the glasses G1, G2 and G3 due to finer scale morphology and a relatively lower volume fraction of the droplets.

Infrared (FTIR) spectra of the experimental glasses G1, G3 and $L_{23}S_{77}$ are plotted in Fig. 2. All samples show lack of sharpness and a broad band in the region 850–1300 cm^{-1}. Two smaller absorption bands can be observed at ∼470 (a) and ∼800 cm^{-1} (b).

Some properties of experimental glasses are presented in Table 2. The transition points (T_g) and softening points (T_s) for the investigated glasses ranged between 477–498 and 501–537 °C, respectively. Glass G1 exhibits the highest T_g and T_s, while the lowest is shown by glass $L_{23}S_{77}$. The measured CTE (200–400 °C) values for the glasses $L_{23}S_{77}$, G1, G2, and G3 were 8.16, 8.47, 8.69 and 9.65 ($\times 10^{-6}$ K^{-1}), respectively. Consequently, an increase in Al_2O_3 and K_2O in the as-investigated proportions favours the decrease in CTE and increase in T_g and T_s of the glasses. These results are in accordance with our earlier study,[16] while some discrepancies in the CTE values might be

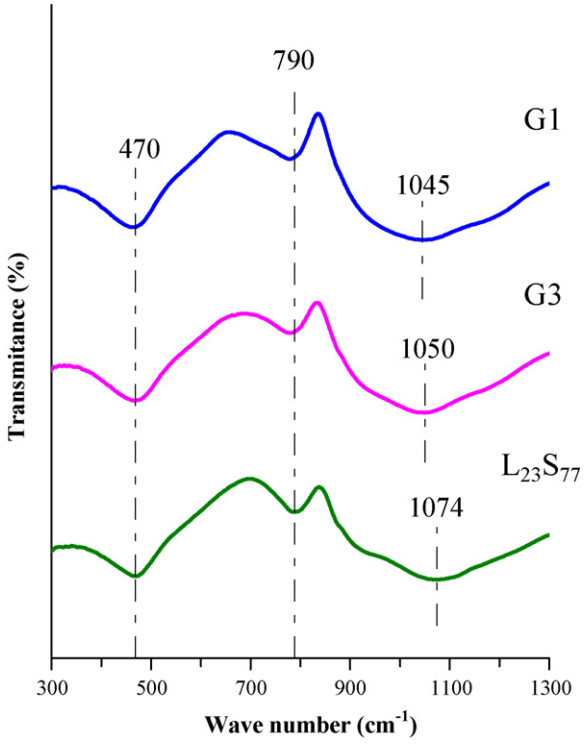

Fig. 2. FTIR spectra of the non-annealed bulk glasses G1, G3 and $L_{23}S_{77}$.

attributed to differences in the preparation of glasses (using Pt crucibles in this study) and in the annealing procedures.

Density of glass $L_{23}S_{77}$ was 2.31 g cm^{-3} while for other glasses the measured density was 2.36 g cm^{-3}. It was observed that molar volume (V_m), oxygen molar volume (V_o) and excess molar volume V_e (calculated using density values of annealed glasses[16]) diminished with decreasing Al_2O_3 and K_2O content as well as SiO_2/Li_2O content in the glasses (Table 2). It is worthy noting that no significant differences were observed in the values of V_m, V_o and V_e for annealed and non-annealed glasses.

3.2. Crystallization of bulk glasses

The changes in the appearance of monolithic glasses after heat treatment at 550, 650, 750, 800 and 900 °C for 1 h is presented in Table 3. Fig. 3 presents the DTA thermographs for all the investigated glasses at $\beta = 15$ K min^{-1}. As is evident from Fig. 3, the exothermic crystallization peaks for the G1 and G2 glasses were significantly less pronounced in comparison

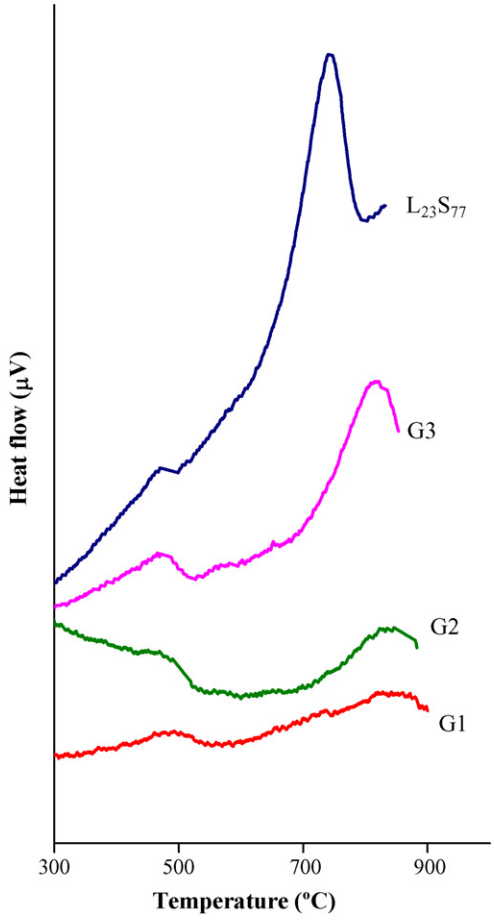

Fig. 3. DTA thermographs for all the investigated glasses at $\beta = 15$ K min^{-1}.

to those of G3 and $L_{23}S_{77}$ compositions. Using lower heating rates of 2, 5 and 10 K min^{-1}, the tendency is the same, i.e., the crystallization peaks for the glasses G1 and G2 could be hardly distinguished, while the glasses G3 and $L_{23}S_{77}$ exhibit sharp exothermic crystallization peaks under the same experimental conditions (not shown). The values of T_p for glasses $L_{23}S_{77}$, G3, G2 and G1 are 749, 823, 835 and 831 °C, respectively, and T_p tends to shift towards higher temperatures with increasing heating rates.

Fig. 4 presents the evolution of phases in bulk glasses heated at different temperatures for 1 h. No crystallization events could be detected by XRD analysis in G1, G2 and G3 at both 550 and 650 °C while strong peaks of LD with quartz (Q) traces were already registered in $L_{23}S_{77}$ at 650 °C. The same phase

Table 2
Properties of the experimental glasses.

	$L_{23}S_{77}$	G1	G2	G3
Density (g cm^{-3})	2.31 ± 0.01	2.36 ± 0.01	2.36 ± 0.01	2.36 ± 0.01
NBO/T	0.60	0.36	0.47	0.60
T_g (°C)	477	498	495	477
T_s (°C)	501	537	531	514
$CTE_{200–400\ °C}$ (10^{-6} K^{-1})	8.16	8.47	8.69	9.65
Molar volume (cm^3 mol^{-1})	23.02 ± 0.01	25.24 ± 0.01	24.27 ± 0.02	23.38 ± 0.01
Oxygen mol. vol. (cm^3 mol^{-1})	13.90 ± 0.01	15.14 ± 0.02	14.85 ± 0.01	14.58 ± 0.01
Excess mol. vol.	1.34 ± 0.01	1.92 ± 0.01	1.53 ± 0.01	1.22 ± 0.01

Table 3
Changes in the appearance of monolithic bulk glasses after heat treatment at different temperatures for 1 h.

	G1	G2	G3	$L_{22}S_{77}$
As-cast glass	Transparent	Transparent	Transparent	Cloudy
450 °C	Transparent	Transparent	Transparent	Cloudy
550 °C	Transparent	Transparent	Semi-transparent	Cloudy
650 °C	Transparent	Transparent	Semi-transparent	White opaline
750 °C	Semi-translucent opaline	White translucent opaline	Semi-translucent opaline	White opaline
800 °C	Semi-translucent opaline	White translucent opaline	White translucent opaline	White opaline
900 °C	Semi-translucent opaline	White translucent opaline	White translucent opaline	White opaque

assemblage was revealed in $L_{23}S_{77}$ upon further heat treating at 750 and 800 °C until 900 °C when cristobalite (C) also appeared. The composition G1 exhibited monomineral Li_2SiO_3 (hereafter referred as LS) as the only crystalline phase at temperatures ≥ 750 °C. In agreement with GC G1, LS crystallized as the only phase in composition G2 after heat treatment at 750 °C. However, with further increase in temperature to 800/900 °C, this crystalline phase was adjoined by LD which precipitated as

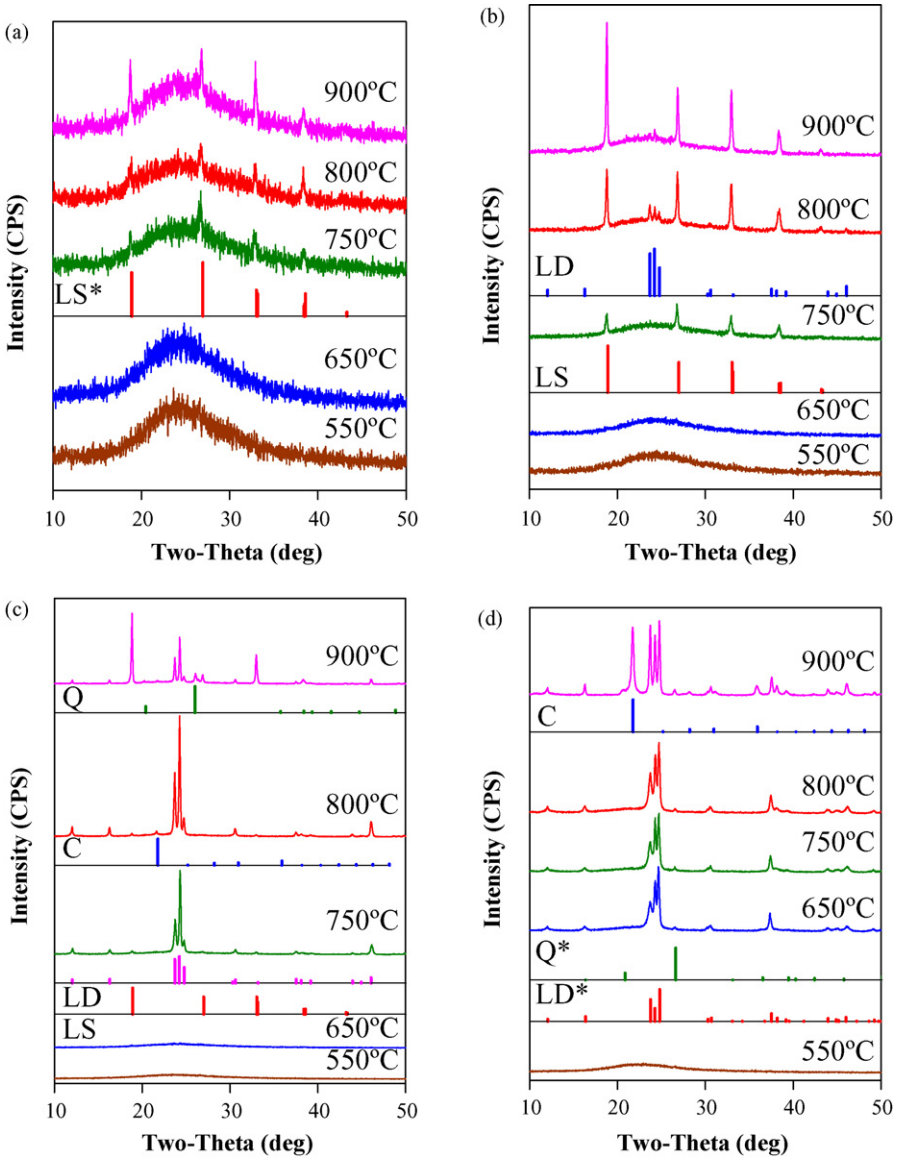

Fig. 4. X-ray diffractograms of bulk glasses heat treated at 550, 650, 750, 800 and 900 °C: (a) G1, (b) G2, (c) G3 and (d) $L_{23}S_{77}$. LS*: lithium silicate (Li_2SiO_3, ICCD card 01-070-0330); LS: lithium silicate (Li_2SiO_3, ICCD card 00-029-0828); LD*: lithium disilicate ($Li_2Si_2O_5$, ICCD card 01-072-0102); LD: lithium disilicate ($Li_2Si_3O_5$, ICCD card 01-049-0803); *Q*: quartz (SiO_2, ICCD card 01-070-2516); *Q**: quartz (SiO_2, ICCD card 01-077-1060); C: cristobalite (SiO_2, ICCD card 01-082-0512) [scale bar: (a) 3500, (b) 3500, (c) 70,000 and (d) 40,000 cps].

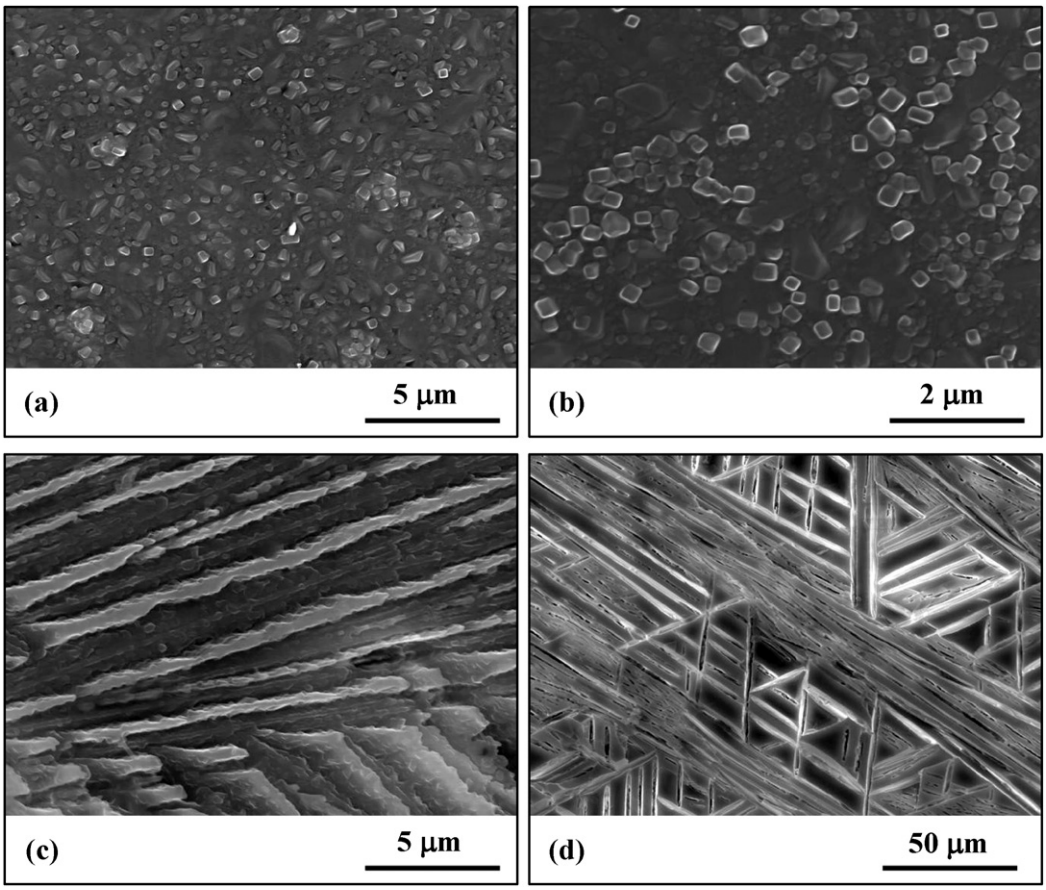

Fig. 5. SEM images of glass G3 heat treated at several temperatures: (a) 550, (b) and (c) 750, and (d) 900 °C.

a secondary phase. The composition G3 with lowest K_2O and Al_2O_3 content exhibited LD as the major phase formed at 750 °C together with traces of LS.

Surface crystallization and dendritic skeletal crystal growth of LS could be observed by SEM in both G1 and G2 in the temperature interval 750–900 °C (not shown), being consistent with nucleated droplet phase separation in the inner part of the specimens as previously documented for glass G1.[16] SEM images of G3 support the conclusion that LD crystal growth occurred in the form of rods upon heat treating in the temperature interval of 550–750 °C (Fig. 5(a) and (b)), nucleated from the nanosize droplet phase revealed in the parent non-annealed glass (Fig. 1). G3 specimens became semi-transparent at 550 °C (Table 3) before any crystallization could be detectable by XRD. These results suggest that the volume fraction of crystals developed was less than the limit of XRD resolution.[24] Apart from the individual fine rod like crystals observed in the core of G3 specimen at 750 °C (Fig. 5(b)), there was a structural rearrangement trend towards the formation of oriented fibres (Fig. 5(c)). This is consistent with optical observations made by Morse and Donnay[25] who concluded that the size increase of LD crystals occurs through nucleation and growth of individual rods because every point of the surface of growing fibre can act as a nucleating site for a new rod. Crystal growth of LD in G3 resulted in the formation continuous laminar fibres of LD at 900 °C (Fig. 5(d)).

The SEM images of heat treated $L_{23}S_{77}$ specimens show that the nuclei growth up to the critical size at 550 °C (Fig. 6(a)) has been followed by the formation of LD spherulites at 650 °C (Fig. 6(b)) as detected by XRD (Fig. 4(d)). At elevated temperatures, 750 and 800 °C, spherulites were composed by numerous submicron roundly shaped crystals (Fig. 6(c)) followed by a coarsening process at 900 °C (Fig. 6(d)) with simultaneous formation of cristobalite, as identified by XRD analysis (Fig. 4(d)). Seemingly $L_{23}S_{77}$ was almost fully crystallized at 800 °C and then residual silica rich glass phase start to devitrify in the form of cristobalite.

Crystallization kinetics studies were performed only for glasses G3 and $L_{23}S_{77}$ because glasses G1 and G2 showed low tendency towards devitrification and exhibited negligible crystallization exothermic curves at the experimental heating rates ($\beta = 2$–$15\ \mathrm{K\ min^{-1}}$) used in this study. It may be observed that $\left.\frac{d\chi}{dt}\right|_p$ increases with the heating rate (Fig. 7, Eq. (2)). The plots of crystallization fraction vs temperature show that crystallization rate of LD decreases with addition of Al_2O_3. This can be attributed to a longer time duration required for the minimum percentage of crystallinity to be detectable by XRD.[24,26] The values of E_c for glasses $L_{23}S_{77}$ and G3 are 153 and 330 kJ mol^{-1}, respectively while the value of n is $\sim 3.04 \pm 0.05$ and 1.51 ± 0.02, respectively. The corresponding mean values may be taken as the most probable quoted exponents.

3.3. Crystallization of glass powder compacts

The variations in density, shrinkage and bending strength of glass powder compacts with firing temperature in the range 800–900 °C are plotted in Fig. 8. Well densified GC-materials G1 and G2 exhibiting bending strength values of 114 ± 2 and 158 ± 5 MPa, respectively, were obtained after sintering at 800 °C (Fig. 8, Table 4). Under the same conditions, GC3 featured lower mechanical properties (81 ± 8 MPa) in comparison to GC1 and GC2, while $L_{23}S_{77}$ samples exhibited high fragility and the lowest values of flexural strength (0.7 ± 0.1 MPa) and density (2.03 ± 0.05 g cm^{-3}) among all investigated compositions. No improvement in densification level was observed for this Al_2O_3 and K_2O free composition after further heat treatment, resulting in mechanically very weak and highly porous samples. On the contrary, GC3 demonstrated the beneficial effect of small addition of Al_2O_3 and K_2O to bicomponent composition $L_{23}S_{77}$. In particular, increases of density (2.25 ± 0.01 g cm^{-3}), shrinkage ($15.9 \pm 0.3\%$) and mechanical strength (216 ± 3 MPa) were observed after firing at 850 °C followed by further densification and strengthening at 900 °C (density 2.36 ± 0.01 g cm^{-3}, bending strength 224 ± 4 MPa). The GCs from glass G1 and G2 showed the maximum density values (2.34 and 2.36 g cm^{-3}, respectively) at 850 °C followed by a smooth decrease at 900 °C. Their maximum flexural strength values of 189 ± 8 MPa for composition GC1 and of 195 ± 9 MPa for composition GC2 were attained at 900 °C.

X-ray diffractograms revealed LS as the single crystalline phase in GC1 after sintering at 800 °C (Fig. 9), while GC2 and GC3 comprised LS along with *Q* and LD as minor phases (Fig. 9(b) and (c)). At 850 and 900 °C (Fig. 9(c)), GC3 featured almost monomineral composition of LD with peaks of low intensity attributed to *Q*. From the XRD spectra of the compositions with higher amount of Al_2O_3 and K_2O LD was revealed in G1 and became principle phase in G2 after sintering at 850 °C. Finally, LD was the main crystalline phase while LS and Q were minor phases in both GC1 and GC2 at 900 °C.

LD was the main crystalline phase in $L_{23}S_{77}$ glass powder compacts sintered at 800 and 850 °C (Fig. 9(d)). Most probably, GC $L_{23}S_{77}$ was almost fully crystallized at 800 °C. Then, the residual glassy phase depleted from lithium and having high silica content starts to crystallize in the form of quartz and tridymite.[27] Finally, quartz along with LD became the principal crystalline phases at 900 °C and peaks of tridymite along with cristobalite were also observed in the XRD pattern (Fig. 9(d)) which is, in fact, in good correlation with phase diagram of SiO_2–Li_2O binary system.[28]

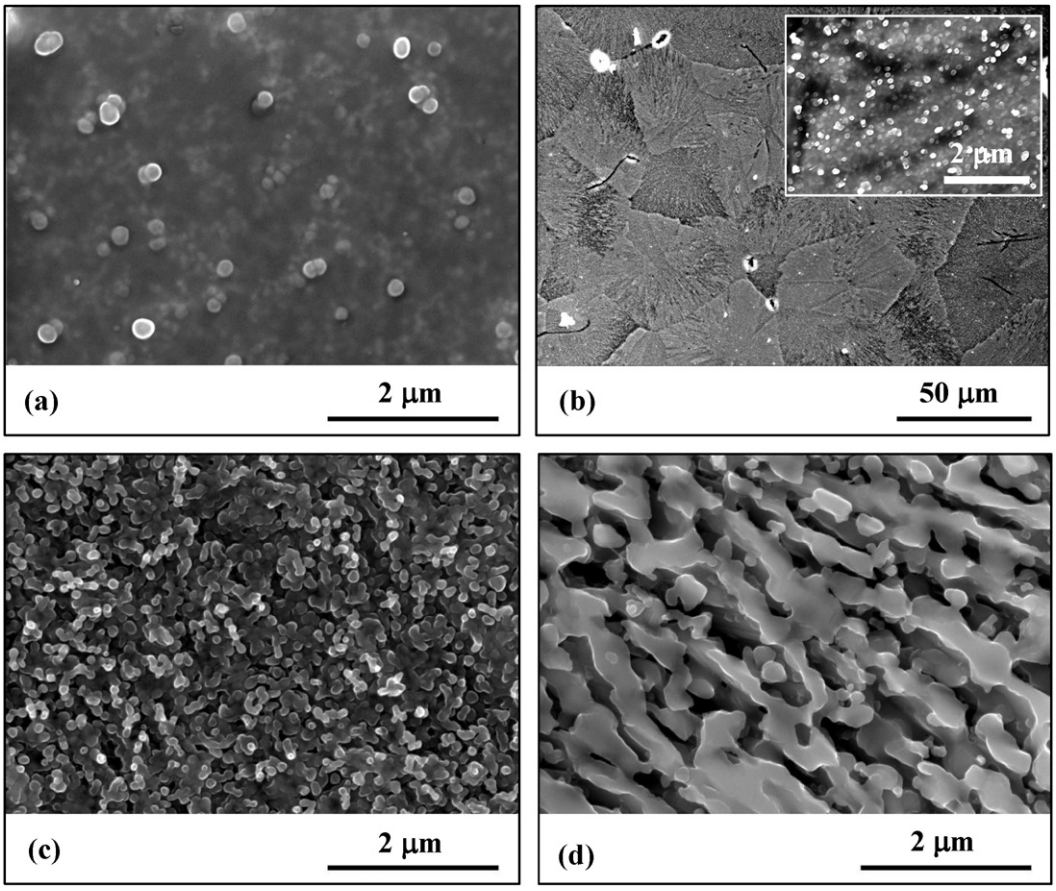

Fig. 6. SEM images of glass $L_{23}S_{77}$ heat treated at several temperatures: (a) 550, (b) 650, (c) 800, and (d) 900 °C.

Table 4
Properties of the glass powder compacts heat treated at different temperatures.

	$L_{23}S_{77}$	G1	G2	G3
Density ($g\,cm^{-3}$)				
800 °C	2.03 ± 0.05	2.28 ± 0.05	2.35 ± 0.01	2.19 ± 0.03
850 °C	2.04 ± 0.07	2.34 ± 0.01	2.36 ± 0.01	2.25 ± 0.01
900 °C	2.14 ± 0.04	2.33 ± 0.01	2.35 ± 0.01	2.36 ± 0.01
Shrinkage (%)				
800 °C	0.7 ± 0.1	17.0 ± 0.3	16.9 ± 0.1	12.6 ± 0.1
850 °C	1.7 ± 0.2	17.9 ± 0.2	17.1 ± 0.1	15.9 ± 0.3
900 °C	5.2 ± 0.1	18.1 ± 0.1	17.2 ± 0.1	18.0 ± 0.3
Bending strength (MPa)				
800 °C	0.7 ± 0.1	114 ± 2	158 ± 5	81 ± 8
850 °C	1.0 ± 0.2	134 ± 4	187 ± 14	216 ± 3
900 °C	13 ± 2	189 ± 8	195 ± 9	224 ± 4
$CTE_{200–500\,°C}$ ($10^{-6}\,K^{-1}$)[a]	13.45	7.41	7.91	8.69
$CTE_{200–700\,°C}$ ($10^{-6}\,K^{-1}$)[a]	12.51	9.00	9.57	9.94

[a] Samples sintered at 900 °C.

The microstructures of the GC1, GC2 and GC3 observed under SEM revealed different morphologies of the crystals developed. The typical microstructure of GC1 sintered at 800 °C (Fig. 10(a)) features dendrite configuration of LS crystals in SiO_2–Li_2O system.[28] Heat treatment of G1 at 850 °C made LD crystals to grow in the form of submicron sized rods that act as nucleating sites for new rods that increase in size (Fig. 10(b)). Crystal growth of the individual LD rods in G2 and G3 at 900 °C resulted in the formation of continuous lam-

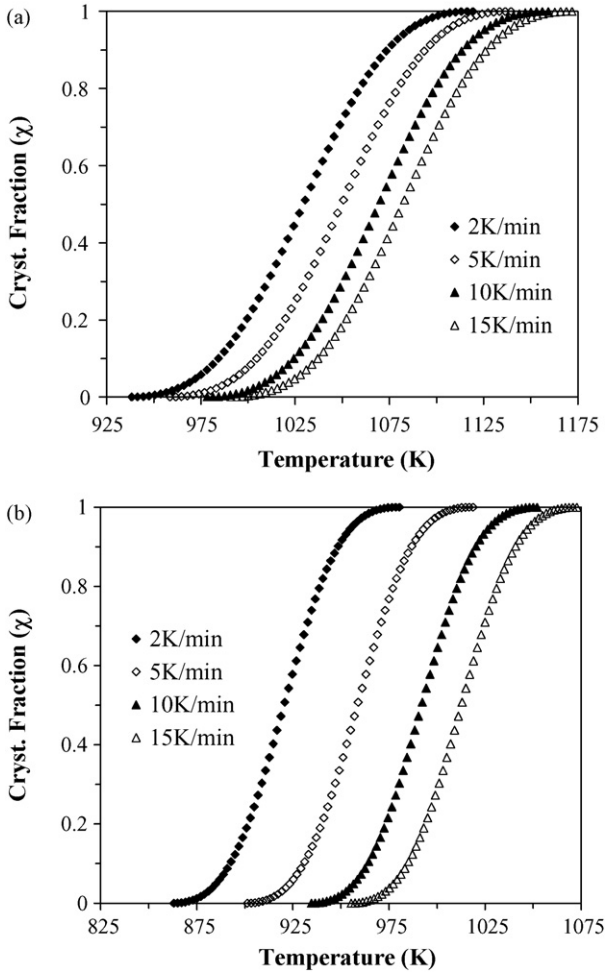

Fig. 7. Crystallization fraction vs heat treatment temperature: (a) G3 and (b) $L_{23}S_{77}$.

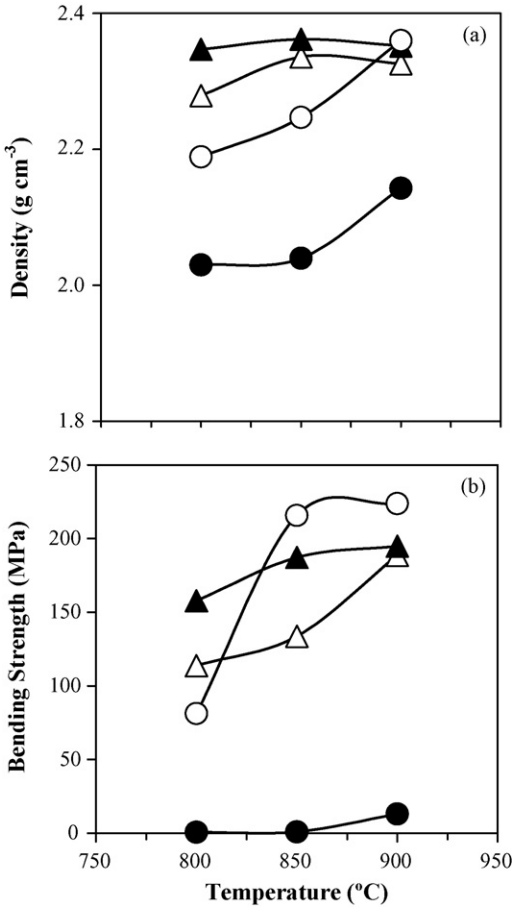

Fig. 8. Some properties of glass powder compacts heat treated at different temperatures: (a) density and (b) bending strength [●: $L_{23}S_{77}$; △: G1; ▲: G2; ◯: G3].

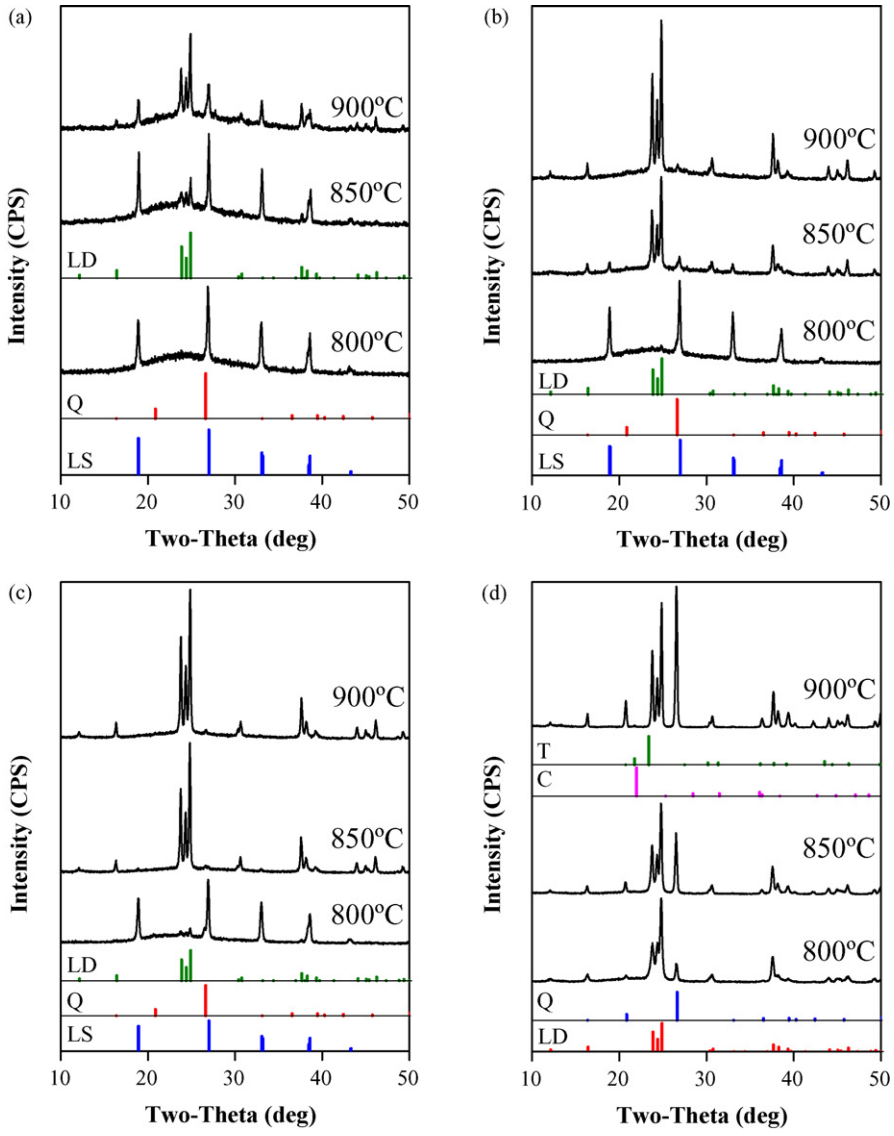

Fig. 9. X-ray diffractograms of glass powder compacts heat treated at 800, 850 and 900 °C: (a) G1, (b) G2, (c) G3 and (d) $L_{23}S_{77}$. LS: lithium silicate (Li_2SiO_3, ICCD card 01-070-0330); LD: lithium disilicate ($Li_2Si_2O_5$, ICCD card 01-070-4856); *Q*: quartz (SiO_2, ICCD card 01-077-1060); T: trydimite (SiO_2, ICCD card 00-042-1401); C: cristobalite (SiO_2, ICCD card 00-039-1425) [scale bar: (a) 12,500, (b) 18,500, (c) 28,000 and (d) 45,000 cps].

inar fibres of LD embedded in glassy matrix (Fig. 10(c) and 10(d)) which are responsible for high mechanical strength of these GCs.

Fig. 11 reveals two main steps of sintering for glass powder compacts G1, G2 and G3 during a thermal treatment at a constant heating rate (5 K min^{-1}) from ambient temperature to 1000 °C. Since glass G3 has lower T_g, it starts to sinter earlier than glass G1 and G2 exhibiting the temperature of first initial shrinkage T_{FS1} at 525 °C. The first maximum shrinkage (T_{MS1}) for glass G3 was assigned at 570 °C that was well correlated with first signs of LS crystallization at 550 °C evidencing from the XRD analysis (not shown). Thus, the interval of first sintering step was wider for G1 (68 °C) and for G2 (49 °C) in accordance with their higher T_p values. As soon as the first sintering period finishes, LS start to precipitate from the glass reservoir and crystallization becomes the dominant process. No shrinkage occurs during this period since crystallization impedes densification. A second shrinkage stage starts almost synchronically at 793–795 °C for all experimental compositions, the maximum shrinkage (T_{MS2}) being reached at 851, 822 and 924 °C for G1, G2 and G3, respectively.

4. Discussion

4.1. Bulk glasses

According to Vogel,[9] liquids in pure Li_2O–SiO_2 system containing less than 30 mol.% Li_2O undergo phase separation into droplet like zones of Li-rich phase and SiO_2-rich glass matrix within a metastable immiscibility dome.[29] Consequently, the cloudy appearance of the $L_{23}S_{77}$ glass was expected. Moreover,

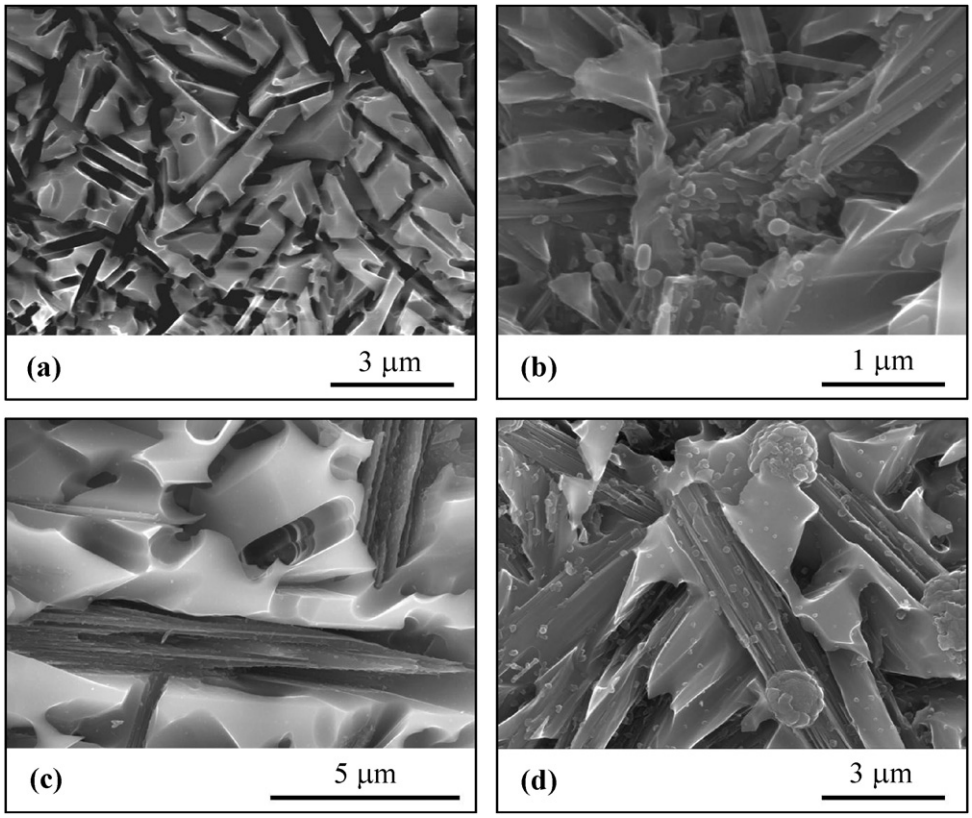

Fig. 10. SEM images of heat treated glass powder compacts: (a) G1, 800 °C; (b) G1, 850 °C; (c) G2, 900 °C; and (d) G3, 900 °C.

the droplet size in this glass has remained nearly the same as observed by Vogel.[9]

SEM examination of the segregation effects occurring in bulk glasses (Fig. 1) confirms that incorporation of Al_2O_3 greatly decreases the immiscibility trend. This phenomenon can be explained by the structural role of Al^{3+} which may exist in four coordinated position due to the presence of alkali cations in the glasses. In order to maintain local charge neutrality, $(AlO_{4/2})^-$ units will be charge compensated by alkali cations (K, Li) which must be present in the vicinity of each such tetrahedron. Therefore, the $(AlO_{4/2})^-$ tetrahedra will substitute directly into the network for silicon-oxygen tetrahedra and simultaneously tend to suppress the immiscibility while raising the T_g and decreasing the CTE of glasses.[16,29]

The lack of sharpness featured in FTIR spectra of the experimental glasses G1, G3 and $L_{23}S_{77}$ (Fig. 2) is indicative of the general disorder in the silicate network mainly due to a wide distribution of Q^n units (polymerization in the glass structure, where n denotes the number of bridging oxygens) occurring in these glasses. The broad absorption band in the higher wave number region (850–1300 cm^{-1}) is attributed to the stretching vibrations of $[SiO_4]$ tetrahedra. The bands at ~470 and ~800 cm^{-1} are linked to bending modes of the silicate network.[30] The FTIR stretching band of SiO_2 tetrahedra slightly broadened in $L_{23}S_{77}$ in comparison with Al_2O_3-containing glasses G1 and G3. Additionally, the appearance of absorption bands at frequencies ~870, ~915 cm^{-1} in $L_{23}S_{77}$ proves existence of broader distribution of the non-bridging oxygens among the tetrahedral cation and a less polymerized glass network. On the contrary, a shallow band at frequency ~1170 cm^{-1} was observed in the infrared spectra of Al_2O_3-containing glasses, in particular G1 suggesting towards the occurrence of Q^4 units and consequently an increase in cross-linking degree. Nevertheless, further ^{27}Al-MAS-NMR study will be performed to support the hypothesis of Al incorporation in fourfold coordination and its homogeneous mixture within the silicate matrix.

Based on the assumption that Al^{3+} acts as a network former, the numbers of non-bridging oxygen per each tetrahedral cation (NBO/T) were calculated[31] for the glasses G1, G2, G3 and $L_{23}S_{77}$ as 0.36, 0.47, 0.60 and 0.60, respectively (Table 2), suggesting more polymerized glass network structures for G1 and G2. Moreover, from Table 2, G1 exhibits the highest T_g while the lowest T_g values are shown by the G3 and $L_{23}S_{77}$ glasses. The addition of Al_2O_3 in proportion corresponding to G1 and G2 decreased the NBO/T and thus, leading to an increase in T_g. This is consistent with the results reported for the effect of RO_n addition on Li_2O–SiO_2–RO_n glasses (R = P, V, Zr).[14,32] On the contrary, the lower T_g values measured for $L_{23}S_{77}$ and G3 (Table 2) can be attributed to a less polymerization extent of the silicate network, i.e., higher number of NBO/T, leading to a lower viscosity. At a given temperature, the viscosity of binary silicate melts and super cooled melts generally decreases with increasing concentration of modifiers and NBO/T.[33]

Al^{3+} essentially acts as network former, thus, increasing the molar volume of the glasses G1 and G2. The V_m and V_o values for glass the G3 were higher than for the glass $L_{23}S_{77}$ while an

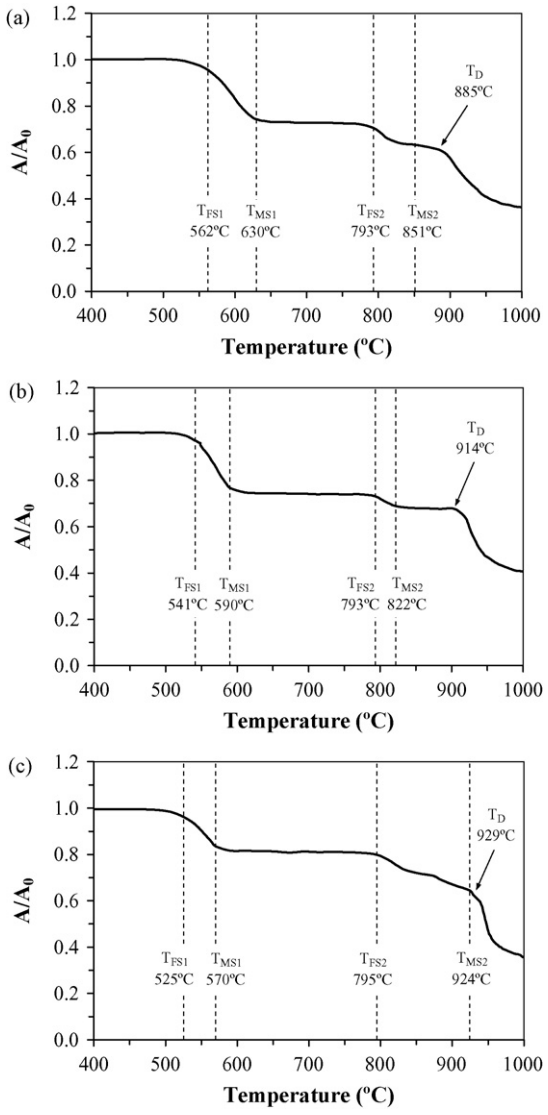

Fig. 11. Variation in relative area (A/A_0: A_0 is the initial area at room temperature, A is the area at defined temperature) powder samples (a) G1, (b) G2 and (c) G3 during the HSM measurement.

opposite trend was observed for V_e. The lower V_e value for glass G3 in comparison to glass $L_{23}S_{77}$ is likely due to the collapse of the structural skeleton into a closer packing because of the presence of two highly ionic oxides (K_2O and Li_2O) in the former which further leads to higher CTE of glass G3 in comparison to glass $L_{23}S_{77}$.

The peak temperature of crystallization (T_p) tendency to shift towards higher temperatures with addition of Al_2O_3 and K_2O can also be attributed to the structural role of the Al_2O_3 having glass forming units $(AlO_{4/2})^-$ that are larger than $(SiO_4)^{-4}$ tetrahedra due to the different ionic radius of Al^{3+} (0.53 Å) and Si^{4+} (0.40 Å).[34] This leads to an increasing viscosity of the glasses, further reducing the mobility of the different ions and ionic complexes operative in the crystallization process. This result is in good agreement with XRD data and SEM observations of the heat treated specimens.

The Avrami parameter for both the glasses $L_{23}S_{77}$ and G3 suggests bulk crystallization with constant number of nuclei, i.e., the existence of three-dimensional bulk crystallization that is diffusion controlled in the case of G3.[35,36] The higher E_c for glass G3 in comparison to glass $L_{23}S_{77}$ reflects the structural role of Al_2O_3 in the investigated compositions and supports the explanation presented above. The E_c value for glass $L_{23}S_{77}$ (153 kJ mol^{-1}) was lower in comparison to that obtained by Freiman and Hench[24] (205 kJ mol^{-1}) for a glass with the composition $25Li_2O$–$75SiO_2$ (mol.%). This difference might be due to different compositions and approaches used to investigate crystallization kinetics.

4.2. Glass powder compacts

Significant changes in crystalline phase assemblage of Al_2O_3 and K_2O containing GCs occurred in the temperature interval of 800–900 °C. LD precipitated as a secondary phase in GC1 after heat treatment at 850 °C along with quartz (*Q*) and LS as major crystalline phases. However, after heat treatment at 900 °C, LD crystallized to be the primary phase in GC1 along with *Q* and LS as secondary phases. It is noteworthy LD was not recorded in GC1 prepared through nucleation and crystallization approach in monolithic bulk glasses. This behaviour can be ascribed to the difference in preparation routes of the parent glasses as water quenching of the glass increases the OH content. The hydroxyl groups may act as a modifier and break the silicate network, thus, reducing the viscosity and activation energy of viscous flow.[16,37] A large fraction of LD precipitated out to become the major phase in GC2 and GC3 after sintering at 850 and 900 °C. Crystallization of LD during preparation of glass-powder compacts G1, G2 and G3 predominantly occurs at temperatures above 800 °C via the precursor LS phase[16,38] due to the reaction described by the following chemical equation

$$Li_2SiO_3 + SiO_2 \rightarrow Li_2Si_2O_5 \quad (3)$$

No aluminium and potassium associated phases were found by XRD analysis in GC1, GC2 and GC3, resulting in improved mechanical strength compared to data obtained for GCs in the previous study.[16]

For the GC1, GC2 and GC3 the CTE values were higher within the range of 200–700 °C than within the range of 200–500 °C (Table 4), but the difference is smaller in case of GC3, compared to GC1 and GC2, most probably due to its lower amount of quartz. The phase inversions of silica polymorphs are completely reversible on cooling and in particular volume changes of tridymite and cristobalite occur at lower temperature than that of quartz when stress relief due to viscous flow in the residual glass phase cannot take place. These changes cause greater stresses during heating and cooling through the inversion temperature ranges leading to weakening of the material. Nevertheless, the main reason for low mechanical performance of $L_{23}S_{77}$ GC was its poor sintering ability due to an early initiation of devitrification process in comparison to Al_2O_3 and K_2O containing glasses. In general, the desired order of events in glass-powder densification process occurs when sintering

precedes crystallization. Hence, glasses with large temperature interval between T_g and T_c can possibly be well sintered.[39] When the onset of crystallization occurs before the glass is fully densified, further densification will be impeded by the formation of crystalline phase that increases the matrix viscosity.[40] From the DTA thermographs of glass grains (Fig. 3) the temperature of peak crystallization (T_p), shifted towards higher temperature region with addition of Al_2O_3 and K_2O suggesting an increase in sintering range for experimental compositions in accordance with the trend: $L_{23}S_{77}$ < G3 < G2 < G1. Consequently, the sintering process of $L_{23}S_{77}$ glass powder compacts occurs in narrower T_c–T_g interval compared to Al_2O_3 and K_2O containing compositions and densification was suppressed by the formation of large fraction of LD phase. This phenomenon can explain the behaviour of $L_{23}S_{77}$ that apparently exhibited low flexural strength, density and shrinkage values at 800 °C (Fig. 8, Table 4). Further heat treatment at 850 and 900 °C slightly facilitated densification because the overall volume of the system decreased when residual silica glassy phase (density 2.20 g cm^{-3}) crystallized in the form of quartz (density 2.65 g cm^{-3}) and tridymite (density 2.27 g cm^{-3}). However, the volume changes occurred in the interval 850 and 900 °C were not sufficient to cause appreciable increase of density and mechanical strength. Thus, $L_{23}S_{77}$ sample remained porous and highly fragile even at 900 °C, and densification can only be expected to happen at temperatures close to the liquidus line of SiO_2–Li_2O binary system at which abrupt formation of liquid phase occurs.[41]

Unlike to glass $L_{23}S_{77}$, densification process of glass powder compacts G1, G2 and G3 demonstrated excellent sintering ability although, even these compositions also did not follow the desired sequence of events and sintering was partially impeded by crystallization. However, due to a broader T_c–T_g interval, these glass powder compacts attained significant level of densification before crystallization started. The softening point T_D (the temperature at which the first signs of softening are observed by rounded edges of the samples) and half ball point T_{HB} (the temperature at which the section of the sample forms a semicircle on the microscope grid) increase in the order G3 > G2 > G1.

The viscosity-temperature curves for G1, G2 and G3 glasses can be built considering their dilatometric T_g (log η = 13.3) and the experimental temperatures received from the HSM (first and maximum shrinkage, half ball and fluency). The softening point is very much affected by crystallisation and corresponding viscosity cannot be evaluated. The viscosity data might be fitted to the Vogel–Fulcher–Tamman, VFT, Eq. (4), employing a regressive method with all the viscosity experimental points in the studied range.

$$\log\ \eta = A + \frac{B}{T - T_0} \tag{4}$$

The values of the constants obtained from the fit are the following for each glass (T in °C): G1: A = 1.9699, B = 1072.96, T_0 = 403.763; G2: A = 2.23717, B = 955.356, T_0 = 408.105; G3: A = 2.28236, B = 951.887, T_0 = 390.219.

From the approximate viscosity–temperature curve (Fig. 12) the increasing Al_2O_3 content of the glass has a decisive influence on viscosity. Particularly, glass G3 exhibited lowest viscosity

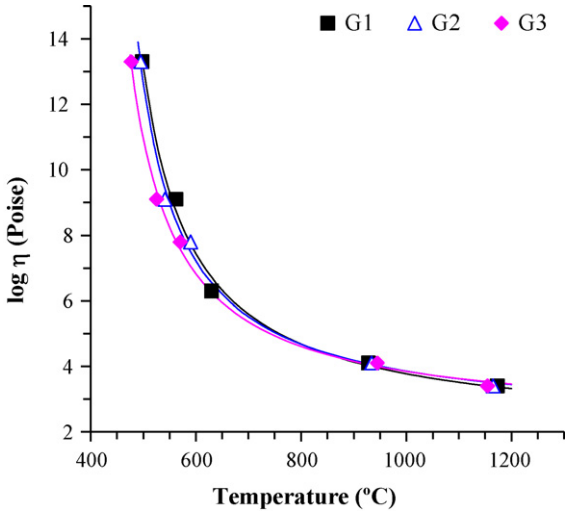

Fig. 12. Viscosity–temperature curve of the experimental glasses.

at temperatures below 850 °C and at the constant temperature log η(G1) > log η(G2) > log η(G3). These results are in accordance with Fluegel[42] reporting that Al_2O_3 usually increases the viscosity of glasses, most significantly at low temperatures, caused by the elimination of non-bridging oxygen sites. Within the scope of optimization of material, Fig. 12 supports our assumption that addition of Al_2O_3 reduces the mobility of the different ions and ionic complexes operative in the nucleation and crystallization process. The opposite trends can be observed when temperatures exceeded 850 °C: compositions G2 and G3 demonstrated higher viscosity than G1. This can be explained by formation of a larger fraction of LD in GC2 and GC3 at 850 °C and 900 °C (Fig. 9(a)–(c)) that cause in shifting of their T_D and T_{HB} values to higher temperature region.

Nevertheless, further quantitative XRD analysis will be required to estimate the amount of glassy phase and its role in the second sintering step of the samples.

5. Conclusions

In context of monolithic bulk glasses, liquid–liquid phase separation occurred in all investigated compositions as illustrated by the nanosize droplets precipitated in the glassy matrixes. Al^{3+} acting as network former decreases the volume fraction and mean diameter of droplet phase resulting in transparent glasses G1, G2 and G3, while the opposite effect was observed in the Al_2O_3 and K_2O free glass that became cloudy on cooling. Surface nucleation and crystallization was dominant in glasses G1 and G2 with LS as the primary crystalline phase while volume nucleation and crystallization was observed in glasses G3 and $L_{23}S_{77}$ with LD as the primary crystalline phase. The values of E_c for glasses $L_{23}S_{77}$ and G3 were 153 and 330 kJ mol^{-1}, respectively.

Sintered glass powder compacts featured enhanced mechanical properties in comparison to materials earlier prepared in alumina crucibles. In compositions with higher amounts of Al_2O_3 and K_2O, both LS and Q were found as minor crystalline phases at 850 and 900 °C, while GC-G3 under the same heat

treatment conditions featured almost monomineral LD composition.

The narrowing of the T_c–T_g interval in the $L_{23}S_{77}$ glass powder compacts in comparison to Al_2O_3 and K_2O containing compositions hindered the densification process and led to the early formation of large fraction of LD phase resulting in poorly densified samples. Small addition of Al_2O_3 and K_2O to pure Li_2O–SiO_2 system enhanced the densification behaviour and the ultimate mechanical strength. Nevertheless, two main steps of sintering were observed by HSM for glass powder compacts G1, G2 and G3, separated by the temperature range within which LS crystallization occurs and temporarily hinders densification.

Acknowledgments

Hugo R. Fernandes is grateful for the financial support of CICECO and for the PhD grant (SFRH/BD/41307/2007) from the FCT, Portugal. Ashutosh Goel is thankful to CICECO and FCT, Portugal (SFRH/BPD/65901/2009) for the post-doctoral research grant.

References

1. James PF, McMillan PW. Quantitative measurements of phase separation in glasses using transmission electron microscopy—1. Experimental technique and method of analysis. *Phys Chem Glasses* 1970;**11**(3): 59.
2. Doremus RH, Turkalo AM. Crystallization of lithium disilicate in lithium silicate glasses. *Phys Chem Glasses* 1972;**13**(1):14.
3. Borom MP, Turkalo AM, Doremus RN. Strength and miscrostructure in the lithium disilicate glass–ceramics. *J Am Ceram Soc* 1975;**58**: 385–91.
4. Headley TG, Loehman RE. Crystallization of glass–ceramics by epitaxial growth. *J Am Ceram Soc* 1984;**67**:620–5.
5. Zanotto ED. Metastable phases in lithium disilicate glasses. *J Non-Cryst Solids* 1997;**219**:42–8.
6. Ota R, Mashima N, Wakasugi T, Fukunaga J. Nucleation of Li_2O–SiO_2 glasses and its interpretation based on a new liquid model. *J Non-Cryst Solids* 1997;**219**:70–4.
7. Ray CS, Day DE, Huang W, Narayan KL, Cull TS, Kelton KF. Non-isothermal calorimetric studies of the crystallization of lithium disilicate glass. *J Non-Cryst Solids* 1996;**204**:1–12.
8. Anspach O, Keding R, Rüssel C. Oriented lithium dicilicate glass–ceramics prepared by electrochemically induced nucleation. *J Non-Cryst Solids* 2005;**351**:656–62.
9. Vogel W. *Structure and crystallization of glasses*. 1st ed. Oxford: Pergamon Press; 1971.
10. Iqbal Y, Lee WE, Holland D, James PF. Crystal nucleation in P_2O_5 doped lithium disilicate glasses. *J Mater Sci* 1999;**34**:4399–411.
11. von Clausbruch CS, Schweiger M, Höland W, Rheinberger V. The effect of P_2O_5 on the crystallization and microstructure of glass–ceramics in the SiO_2–Li_2O–K_2O–ZnO–P_2O_5 system. *Glastech Ber Glass Sci Technol* 2001;**74**:223–9.
12. Wen G, Zheng X, Song L. Effects of P_2O_5 and sintering temperature on microstructure and mechanical properties of lithium disilicate glass–ceramics. *Acta Mater* 2007;**55**:3583–91.
13. Arvind A, Sarkar A, Shrikhande VK, Tyagi AK, Kothiyal GP. The effect of TiO_2 addition on crystallization and phase formation in lithium aluminosilicate (LAS) glasses nucleated by P_2O_5. *J Phys Chem Solids* 2008;**69**(11):2622–7.
14. Lin C, Shen P, Chang HM, Yang YJ. Composition dependent structure and elasticity of lithium silicate glasses. Effect of ZrO_2 additive and the combination of alkali silicate glasses. *J Eur Ceram Soc* 2006;**26**: 3613–20.
15. Rukmani SJ, Brow RK, Reis ST, Apel E, Rheinberger V, Holand W. Effect of V and Mn colorants on the crystallization behaviour and optical properties of Ce-doped Li-disilicate glass–ceramics. *J Am Ceram Soc* 2007;**90**(9):706–11.
16. Fernandes HR, Tulyaganov DU, Goel IK, Ferreira JMF. Crystallization process and some properties of Li_2O–SiO_2 glass–ceramics doped with Al_2O_3 and K_2O. *J Am Ceram Soc* 2008;**91**(11):3698–703.
17. Johnson WA, Mehl KF. Reaction kinetics in processes of nucleation and growth. *Trans Am Inst Mining Eng* 1939;**135**:416–72.
18. Avrami M. Kinetics of phase change. I—general theory. *J Chem Phys* 1939;**7**:1103–12.
19. Avrami M. Kinetics of phase change. II—transformation-time relations for random distribution of nuclei. *J Chem Phys* 1940;**8**:212–24.
20. Avrami M. Kinetics of phase change. III—granulation, phase change, and microstructure. *J Chem Phys* 1941;**9**:177–84.
21. Goel A, Shaaban ER, Ribeiro MJ, Ferreira JMF. Influence of NiO on the crystallization kinetics of near stoichiometric-cordierite glasses nucleated with TiO_2. *J Phys: Condens Matter* 2007;**19**:386231.
22. Pascual MJ, Pascual L, Durán A. Determination of the viscosity–temperature curve for glasses on the basis of fixed viscosity points determined by hot stage microscopy. *Phys Chem Glasses* 2001;**42**:61–6.
23. Pascual MJ, Durán A, Prado MO. A new method for determining fixed viscosity points of glasses. *Phys Chem Glasses* 2005;**46**(5):512–20.
24. Freiman SW, Hench LL. Kinetic of crystallization in Li_2O–SiO_2 glasses. *J Am Ceram Soc* 1968;**51**(7):382–7.
25. Morse HM, Donnay JDH. Optics and structure of three dimensional spherolites. *Am Miner* 1936;**21**(7):391–426.
26. Vázquez J, Wagner C, Villares P, Jiménez-Garay R. Glass transition and crystallization kinetics in Sb0.18As0.34Se0.48 glassy alloy by using non-isothermal techniques. *J Non-Cryst Solids* 1998;**235–237**: 548–53.
27. von Clausbruch CS, Schweiger M, Höland W, Rheinberger V. The effect of P_2O_5 on the crystallization and microstructure of glass–ceramics in the SiO_2.Li_2O–K_2O–ZnO–P_2O_5 system. *J Non-Cryst Solids* 2000;**263/264**:388–94.
28. Höland W, Beall G. *Glass–ceramic technology*. Westerville, OH, USA: The American Ceramic Society; 2002.
29. Shelby JE. *Introduction to glass science and technology*. The Royal Society of Chemistry; 1997.
30. Branda F, Grillo P, Luciani G, Costantini A. Structural role of La_2O_3 in La_2O_3–CaO–Na_2O–SiO_2 glasses Costantini. *Phys Chem Glasses* 2001;**42**:385–8.
31. White WB, Minser DG. Raman spectra and structure of natural glasses. *J Non-Cryst Solids* 1984;**67**:45–59.
32. Matusita K, Sakka S, Maki T, Tashiro M. Study on crystallization of glass by differential thermal analysis. Effect of added oxide on crystallization of Li_2O–SiO_2 glasses. *J Mater Sci* 1975;**10**:94–100.
33. Bansal NP, Doremus RH. *Handbook of glass properties*. San Diego, USA: Academic Press; 1986. p. 223–336.
34. Callister Jr WD. *Fundamentals of materials science and engineering*. New York, USA: John Wiley & Sons; 2001. p. 41.
35. Donald IW. Crystallization kinetics of a lithium zinc silicate glass studied by DTA and DSC. *J Non-Cryst Solids* 2004;**345–346**:120–6.
36. Goel A, Tulyaganov DU, Kansal I, Shaaban ER, Ferreira JMF. Crystallisation kinetics of diopside-Ca-Tschermak based glasses nucleated with Cr_2O_3 and Fe_2O_3. *Int J Mater Eng Innov* 2009;**1**(1):40–60.
37. Cattell MJ, Chadwick TC, Knowles JC, Clarke RL. The crystallization of an aluminosilicate glass in the K_2O–Al_2O_3–SiO_2 system. *Dent Mater* 2005;**21**:811–22.
38. Novaes de Oliveira AP, Manfredini T, Barbiery L, Leonelli C, Pelacani CC. Sintering and crystallization of a glass powder in the Li_2O–ZrO_2–SiO_2 system. *J Am Ceram Soc* 1998;**81**(3):777–80.
39. Silgardi C, DĭArrigo MC, Leonelli C. Sintering behaviour of glass ceramics frits. *Am Ceram Soc Bull* 2000;**9**:88–93.

40. Boccaccini AR, Stumpfe W, Taplin DMR, Ponton CB. Densification and crystallization of glass powder compacts during constant heating rate. *Mater Sci Eng* 1996;**A219**:26–31.
41. Tulyaganov DU, Agathopoulos S, Fernandes HR, Ventura JM, Ferreira JMF. Crystallization of glasses in the system tetrasilicic mica-fluorapatite-diopside. *J Eur Ceram Soc* 2004;**24**(13): 3521–8.
42. Flugel A. Glass viscosity calculation based on a global statistical modelling approach. *Glass Technol: Eur J Glass Sci Technol* 2007;**48**(1):13–30.